Electrochemical Lithography

DOI: 10.1002/anie.201204801

Electrochemical X-ray Photolithography**

Andrei A. Eliseev, Nina A. Sapoletova, Irina Snigireva, Anatoly Snigirev, and Kirill S. Napolskii*

Recent progress in information technologies has made micro- and nanolithography key processes in modern industry. Today these methods are among the most rapidly developing areas in both science and engineering. In the last two decades, well-known and widespread methods of photo- and electron-beam lithography have been complemented by a number of novel approaches that include direct writing processes, such as scanning probe lithography and dip-pen nanolithography, mask-based techniques including soft-lithography, nanoimprint, nanostencil and nanosphere lithography, and unconventional wet lithographies.[1] Progress in the development of these methods has allowed high throughput to be attained at an ultimate resolution of less than 10 nm and enabled mass-production of microelectronic components. Further improvements in this method were introduced by the addition of chemical transformations, which can be applied through the integration of lithography with chemical or electrochemical processes.[2,3]

Electrochemical processing possesses a number of important advantages, including room-temperature synthesis (thereby avoiding thermal expansion problems), ability to control deposition rates, increased deposition density, and enhanced versatility. Moreover, electrochemical processes are easy to control through manipulation of charge values and current transient shapes.[4]

Several electrochemical lithography methods have been reported that achieve resolution down to 10 nm.[2] However, all of these methods require contact lithography processing, as electrochemical photolithographic pattern-transfer techniques have yet to be developed. Nevertheless, numerous papers have been published on light-induced electrochemical effects, which have the potential to be further utilized for the development of non-contact electrochemical lithography techniques.[5,6] One drawback to this approach however, is that the wavelengths of visible and UV light restrict the resolution level. A possible solution to this problem is the use of X-rays, which have long been known to trigger surface charging and radiolysis in matter. It could be expected that these effects would provide the conditions necessary for the electrochemical equilibrium shift required for electrochemical etching or deposition.

Despite this, there have been only a few reports on X-ray-assisted electrochemical processing.[7,8] While some chemical X-ray lithography methods use X-rays for induced chemical transformations, they are restricted to reactions where radiolysis products are formed within the solution volume.[9,10] Some work discusses reactions driven by photoelectrons ejected from the substrate surface, but do not complete the electrochemical circuit to control Helmholtz layer.[11,12] Lastly, we also failed to find any studies concerning direct electrochemical lithography under X-ray irradiation.

Thus in the present study we have focused our attention on the development of an electrochemical X-ray photolithography approach for direct pattern transfer to a liquid–solid interface by coherent X-ray irradiation. The concept is based upon variation in electrochemical deposition/etching rates provided by local photoionization effects. Local reduction of electrolyte components by photoelectrons generated on the working electrode surface under X-rays was chosen to test the concept.

The electrochemical X-ray photolithography method was investigated by pattern transfer onto electrochemically deposited nickel, which plays a pivotal role in industry, particularly in microelectronics. The experiment is shown in Figure 1. A parallel X-ray beam collimated by slits was passed through a 4 μm pitch silicon grating and guided to the

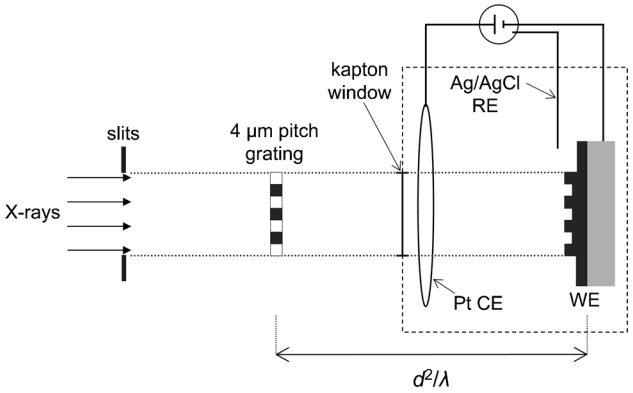

Figure 1. Conceptual plan for electrochemical X-ray photolithography.

[*] Dr. A. A. Eliseev, N. A. Sapoletova, Dr. K. S. Napolskii
Department of Materials Science
Lomonosov Moscow State University
Moscow, 119991 (Russia)
E-mail: eliseev@inorg.chem.msu.ru
Dr. I. Snigireva, Dr. A. Snigirev
European Synchrotron Radiation Facility
Grenoble, 38043 (France)
Dr. K. S. Napolskii
Department of Chemistry, Lomonosov Moscow State University
Moscow, 119991 (Russia)

[**] This work was supported in part by RF President Grant MK-7245.2012.3, by the Russian Foundation for Basic Research (Grant Nos. 11-03-12121 and 10-03-01014), by the Russian Ministry of Education and Science (Grant Nos. 16.513.11.3011, 16.512.11.2164, and 14.740.11.0256) and by M.V. Lomonosov Moscow State University Program of Development. We thank the personnel of the ID06 beamline and, in particular, C. Detlefs for his excellent support. The authors are grateful to G. A. Tsirlina and V. I. Feldman (Moscow State University) for numerous fruitful discussions and to D. I. Petukhov for help with experiments.

Supporting information for this article is available on the WWW under http://dx.doi.org/10.1002/anie.201204801.

electrochemical cell. To create a periodic intensity distribution on the substrate, the distance between the mask and the working electrode was adjusted to the half Talbot distance $Z_T/2 = d^2/\lambda$, where d is the diffraction grating period and λ is the wavelength of X-rays.[13–15]

The idea of combining X-rays with electrochemical processing originated from the experimental observation of increased deposition rate on an illuminated sample area. The thickness of electrodeposited nickel onto a flat Au/Si substrate on the illuminated area of the sample was found to increase substantially compared to the non-irradiated surface. Moreover, an extensive increase in current was observed on switching on X-ray illumination (for details of the electrochemical responses, see the Supporting Information, Figures S1 and S2). The effect of X-ray illumination is observed even under open-circuit conditions, resulting in a slow metal deposition that is pronounced only in long-term experiments (>10 h). The photocurrent increases significantly (10–100 times) when cathodic polarization is applied.

Several effects should be taken into account when describing the processes leading to the variation in deposition rates, including: 1) radiolysis of electrolyte components; 2) photoionization of the electrode surface and electron release into the solution; and 3) redistribution of the charged particles in the electric field. An analysis of absorption cross sections of electrolyte components illustrates that the greatest effect in photoionization is gained by excitation of nickel-containing cations and water molecules (Supporting Information, Table S1). The first ions effectively produce $[Ni(H_2O)_6]^{3+}$, e^-_{aq}, and $OH^\bullet$. Unstable nickel complexes can then further oxidize water to give H_2O_2. Meanwhile, radiolysis of water molecules initiates formation of a number of charged species and free radicals, such as e^-_{aq}, H^+, $H^\bullet$, $OH^\bullet$, H_2O_2, and H_2, with G values decreasing in the order $e^-_{aq} \approx OH^\bullet > H^\bullet > H_2O_2 \approx H_2$.[16] It should be noted that the reaction of free radical $OH^\bullet$ with hydrated nickel(II) cations results in $Ni^{2+}(OH^\bullet)(H_2O)_5$, which is further also converted into $Ni^{3+}{}_{aq}$ in the acidic medium near the cathode.[16] Thus the radiolysis of electrolyte solutions generates nearly equal numbers of highly reactive reducing (e^-_{aq}, $H^\bullet$) and oxidizing ($OH^\bullet$) species. Therefore, as the concentration of hydrated electrons is considerably higher than that of uncharged $H^\bullet$, this effect can be utilized to produce local oxidation/reduction of matter through redistribution of the charged particles in the electric field. Indeed, by applying a potential difference, charged e^-_{aq} species will be pushed off the cathode, while neutral radicals will remain homogeneously distributed in the illuminated area. An excess of $OH^\bullet$ will obviously result in local oxidation of electrodeposited metal at the irradiated parts of the electrode surface by reaction:

$$OH^\bullet + Ni^{\bullet n+} \rightarrow Ni^{n+1} + OH^- \quad (n = 0 - 2) \qquad (1)$$

In the other words, the effects of these processes should decrease deposition rate at the irradiated regions. This mechanism is consistent with radiation-induced potential shifts and corrosion of γ-ray irradiated nickel and its alloys, as demonstrated earlier.[17] However, it strongly contradicts with our observations: the increase in electrodeposited nickel thickness and nickel grain sizes with increasing light intensity (in the areas close to the beam center).

To explain this effect, another established process can be referred to that involves photoionization in the illuminated areas of electrode and an emission of photoelectrons into the electrolyte volume. This mostly applies to secondary electrons, as emission from the core levels is negligible as compared to 5–50 eV electrons. The calculated total absorption of electrode surface layer, electric double layer (EDL), and 100 nm electrode sheath illustrates an excitation efficiency of electrochemical cell components (Table 1). It can be easily seen that the absorption by the electrode surface (5 nm depth) is at least an order of magnitude higher than that of the 100 nm electrode sheath layer. Absorption of a high-energy photon in a metal leads to numerous secondary events with an avalanche-type creation of low-energy excited electrons. In cases the energy of the electron exceeds the Volta potential difference, it can escape from the metal surface to the electrolyte volume. As a result, the photoelectrons ejected from the surface have a wide energy distribution covering the whole energy range from the Volta potential difference to the energy of initial X-rays (12 keV). Generally the dispersion of photoelectrons has a wide maximum at low energies (1–20 eV) and decays dramatically with energy. It should also be noted that the photoelectron inelastic mean free path (IMFP) depends strongly on its energy. Low-energy electrons (<100 eV) have very short IMFPs of <1 nm, while high-energy photoelectrons can escape from the electrode to several nanometers.[18]

Table 1: Total absorption by electrochemical cell components.

Component	t[a] [μm]	ρ[b] [g cm^{-3}]	ω[c] [wt.%]	A_{cs}[d] [cm^2 g^{-1}]	A_{eff}[e] [cm^2 g^{-1}]	A[f] [%]	Products[g]
Ni electrode	0.005[h]	8.9	100	128	128	5.7×10^{-2}	e^-_{aq}
$Ni^{2+}{}_{aq}$ at EDL	0.001	1.13	ca. 10	128	12.8	1.4×10^{-4}	$Ni^{3+}{}_{aq}$, e^-_{aq}
H_2O at EDL	0.001	1.13	ca. 90	2.78	2.5	3×10^{-5}	e^-_{aq}, $OH^\bullet$
$Ni^{2+}{}_{aq}$ at 100 nm	0.1	1.13	3.6	128	4.6	5.2×10^{-3}	$Ni^{3+}{}_{aq}$, e^-_{aq}
H_2O at 100 nm	0.1	1.13	90.7	2.78	2.5	2.9×10^{-3}	e^-_{aq}, $OH^\bullet$
electrolyte	1000	1.13	100	7.83	7.8	58.7	e^-_{aq}, $OH^\bullet$

[a] Effective layer thickness. [b] Density. [c] Mass concentration of component. [d] Absorption cross-section at 12 keV. [e] Effective absorption cross-section. [f] Total absorption. [g] Primary radiolysis products in electrolyte. [h] The data is provided for secondary electrons with an energy of 5–50 eV.

Electron transport from the irradiated area of a metal surface to the electrolyte volume undoubtedly introduces disturbances in the structure of the electric double layer. Most probably, low-energy electrons (with low IMFPs) emitted from the electrode surface reduce the hydrated Ni^{n+} cations in the Helmholtz layer (Figure 2), while high-energy electrons can get through the EDL and reduce Ni cations in the electrolyte volume. The last of these processes results in possible 3D nucleation similar to that observed in radiolysis of

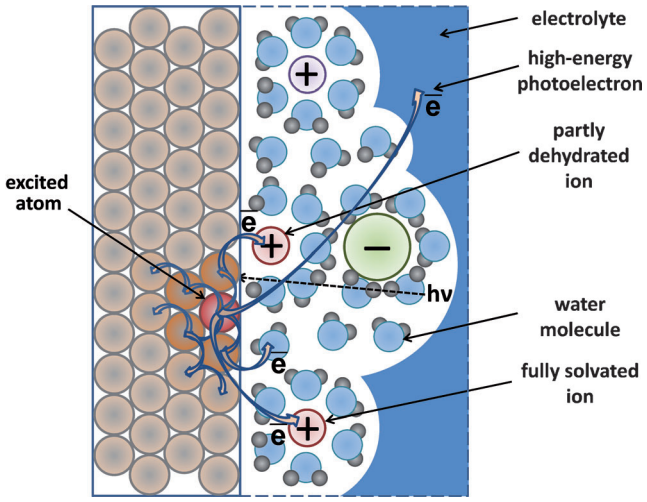

Figure 2. Illustration of the charge transfer during electrochemical X-ray photolithography.

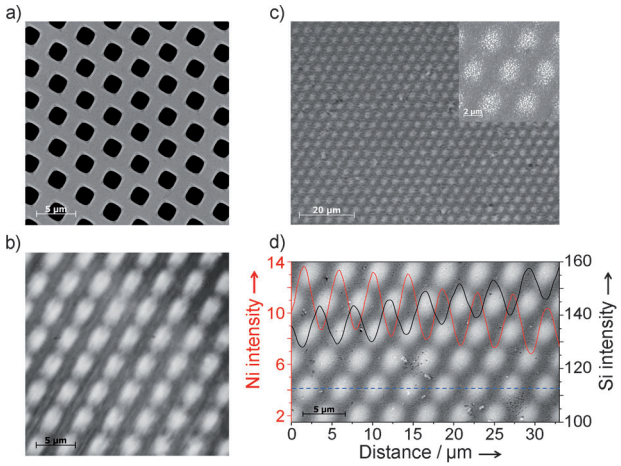

Figure 3. Correspondence between the structure of the lithographic mask and morphology of electrodeposited Ni film. a) Top-view SEM image of the silicon lithographic mask. Scale bar: 5 μm. b) X-ray intensity distribution on the Au/Si substrate, acquired by X-ray transmission microscopy.[20] The lighter regions correspond to areas with a higher intensity of X-ray illumination. Scale bar: 5 μm. c) Top-view SEM image of the nickel electrodeposited onto a Au/Si electrode under periodic X-ray illumination. Scale bar: 20 μm. Inset: magnified image (Scale bar: 2 μm). d) Quantity variation profiles of Ni (red line) and Si (black line) across the blue dashed line depicted on the SEM image of the fabricated Ni grating. Scale bar: 5 μm.

electrolyte solutions;[19] these nuclei can be deposited on the electrode surface or be further dissolved in the electrolyte. In cases where the electrons collide with water molecules, these can also serve as a reducing agent for metal ions. Therefore, emitted electrons generally produce an additional electric current at the electrode–electrolyte interface that involves $Ni^{2+}_{aq} \rightarrow Ni$ transformation, which locally increases the metal electrodeposition rate. Unlike radiolysis products, these electrons have no oxidizing pairs, which obviously shifts the electrochemical equilibrium and enhances deposition rates on the illuminated areas of the electrode. The holes generated by X-rays move to the electrode volume under applied potential difference. The circuit completes through electrochemical reactions on the anode.

Owing to the high charge carrier density and mobility in a metal electrode, the local charging of the electrode provided by photoionization can be neglected. It should be noted that oxidizing radiolysis products and emitted photoelectrons provide opposite effects on the metal deposition rates in the near-cathode region. In the case of high-energy X-rays and effective electrode photoionization, the latter dominate over the oxidation effect of radiolysis products and thus determine the electrochemical equilibrium shift. Low electron inelastic mean free paths in the electrolyte ($\ll 10$ nm) provide high locality of photoelectron reduction of metal cations within the illuminated areas.

To test the feasibility of lithographic processing using X-rays, a periodic illumination of the sample was created using the Talbot effect.[13–15] A silicon grating (Figure 3a) illuminated with collimated coherent light was used to produce a pattern in the transmitted light. If the distance is equal to the Talbot length $2d^2/\lambda$, a self-image of the original structure can be created. At half Talbot length d^2/λ, a self-image of the grating can also occur, but it is laterally shifted by half a period. Typically the contrast in Talbot images decreases with distance from the grating. Consequently, to maximize contrast, a half Talbot length was chosen to produce a pattern with a periodic arrangement of light spots on a darkened surface (Figure 3b).

Figure 3c shows a SEM image of nickel electrodeposited onto an X-ray-illuminated Au/Si electrode. The resulting structure corresponds well to the image of the diffraction grating (Figure 3a); the periodicity of the fabricated Ni pattern (4 μm) is identical to that of the mask. The height of the islands in the resulting structure is clearly dependent on the contrast provided by the self-image of the grating. The EDX mapping of the resulting structure indicates a metal electrodeposition enhancement of up to 150% in the illuminated areas compared to unilluminated regions (Figure 3d). Some unevenness in the resulting element distribution originates from a gradual decrease in the light intensity away from the beam center, thus giving rise to a non-uniform intensity distribution. Moreover, up to 65% variation in nickel quantity is detectable between the nearest bright and dark spots of the image. This indicates an important role for the reducing photoelectron current and its correspondence to direct electrodeposition efficiency.

The proposed electrochemical X-ray photolithography method described herein thus results in a direct non-contact pattern transfer onto an electrodeposited metal film. It should be noted that the short lifetime of radiolysis products, in combination with a small spur radii and electron inelastic mean free paths in condensed matter,[16] provide a possible means to rapidly improve the ultimate resolution of the proposed method to tens of nanometers with further development of X-ray optics. Moreover, regulation of the working electrode potential represents an effective pathway to control deposition rates through variation in ion concentration in the Helmholtz layer. We believe that this electrochemical X-ray photolithography technique presents no limitations for electrochemical processing and can be further expanded to

various technical applications including electrodeposition of metals, semiconductors, and complex structures, X-ray assisted anisotropic electrochemical etching, and other fields that we cannot yet envision.

To summarize, the proposed electrochemical X-ray lithography technique was successfully applied for the creation of a Ni grating by metal electrodeposition under coherent X-ray illumination. The concept is based on a local reducing effect provided by photoelectrons emitted from the electrode surface under X-ray illumination in the electric field. This new approach combines the advantages of X-ray photolithography with the versatility of electrochemical processing and is a novel method for the creation of functional nanostructures.

Experimental Section

The electrochemical X-ray photolithography method was tested by pattern transfer onto an electrochemically deposited nickel film by a parallel X-ray beam. The experiments were performed using the Microoptics test bench at the ID 06 undulator beamline at the European Synchrotron Radiation Facility (ESRF). An X-ray beam with an energy of 12 keV and monochromaticity of $\Delta\lambda/\lambda \approx 10^{-4}$ was collimated by 0.75 mm × 1 mm slits installed at distance of 54.8 m from an undulator light source. The beam, with a total flux of 2×10^{13} photons/s and divergence < 0.4 μrad, was passed through a 4 μm pitch silicon amplitude-phase grating and guided to a three-electrode electrochemical cell with kapton walls, which are nearly transparent to X-rays (12 keV). To create a periodic intensity distribution on the substrate, the mask-to-working electrode distance was adjusted to half of the Talbot length $Z_T/2 = d^2/\lambda$ (see Figure 1).

Si (111) wafers coated by a 100 nm Au layer were used as substrates for metal electrodeposition. The platinum wire counter electrode was aligned at a distance of 3 mm from the sample. The reference electrode was a saturated (KCl) Ag/AgCl electrode connected to the cell by a Luggin capillary. Electrodeposition was carried out in an aerated solution containing 0.6 M $NiSO_4$, 0.1 M $NiCl_2$, and 0.3 M H_3BO_3 at constant $E_d = -0.8$ V versus the reference electrode at room temperature.

Received: June 19, 2012
Revised: August 10, 2012
Published online: October 11, 2012

Keywords: electrochemistry · nickel · photolithography · synchrotron radiation

[1] M. Cavallini, C. Albonetti, F. Biscarini, *Adv. Mater.* **2009**, *21*, 1043 – 1053.
[2] F. C. Simeone, C. Albonetti, M. Cavallini, *J. Phys. Chem. C* **2009**, *113*, 18987 – 18994.
[3] M. Cavallini, F. C. Simeone, F. Borgatti, C. Albonetti, V. Morandi, C. Sangregorio, C. Innocenti, F. Pineider, E. Annese, G. Panaccione, L. Pasquali, *Nanoscale* **2010**, *2*, 2069 – 2072.
[4] N. Sapoletova, T. Makarevich, K. Napolskii, E. Mishina, A. Eliseev, A. van Etteger, T. Rasing, G. Tsirlina, *Phys. Chem. Chem. Phys.* **2010**, *12*, 15414 – 15422.
[5] Y. V. Pleskov, Z. A. Rotenberg in *Adv. Electrochem. Electrochem. Eng.*, *Vol. 11* (Eds.: H. Gerischer, C. W. Tobias), Wiley, New York, **1978**, pp. 1 – 124.
[6] N. M. Alpatova, L. I. Krishtalik, Y. V. Pleskov, in *Top. Curr. Chem.*, *Vol. 138* (Eds.: M. J. S. Dewar, et al.), Springer, Berlin, **1987**, p. 149.
[7] Q. Ma, N. Moldovan, D. C. Mancini, R. A. Rosenberg, *J. Appl. Phys.* **2001**, *89*, 3033 – 3040.
[8] V. Kaajakari, US, WO/2008/080004, **2008**.
[9] R. Divan, D. C. Mancini, N. Moldovan, L. Assoufid, Y. S. Chu, Q. Ma, R. A. Rosenberg, *Proc. Int. Conf. Semicond.*, Sinaia, Romania, **2003**, pp. 39 – 42.
[10] R. Divan, Q. Ma, D. C. Mancini, D. T. Keane, *Rom. J. Inform. Sci. Tech.* **2008**, *11*, 71 – 84.
[11] Q. Ma, R. Divan, D. C. Mancini, R. A. Rosenberg, J. P. Quintana, D. T. Keane, *Appl. Phys. Lett.* **2006**, *89*, 083114.
[12] P. C. Hsu, C. H. Wang, T. Y. Yang, Y. K. Hwu, C. S. Lin, C. H. Chen, L. W. Chang, S. K. Seol, J. H. Je, G. Margaritondo, *J. Vac. Sci. Technol. A* **2007**, *25*, 615 – 620.
[13] H. F. Talbot, *Philos. Mag.* **1836**, *9*, 401 – 407.
[14] L. Rayleigh, *Philos. Mag.* **1881**, *11*, 196 – 205.
[15] P. Cloetens, J. P. Guigay, C. De Martino, J. Baruchel, M. Schlenker, *Opt. Lett.* **1997**, *22*, 1059 – 1061.
[16] J. H. Baxendale, F. Busi, *Proceedings of the NATO Advanced Study Institute*, Capri, Italy, 7 to 18 September **1981**.
[17] N. Y. Bune, Y. M. Kolotyrkin, G. S. Tyurikov, *Zh. Fiz. Khim.* **1958**, *32*, 2679 – 2685.
[18] M. P. Seah, W. A. Dench, *Surf. Interface Anal.* **1979**, *1*, 2 – 11.
[19] A. Henglein, *J. Phys. Chem.* **1993**, *97*, 5457 – 5471.
[20] A. Bosak, I. Snigireva, K. S. Napolskii, A. Snigirev, *Adv. Mater.* **2010**, *22*, 3256 – 3259.

